Vol. 46, No. 3 (2024) 526-534, DOI: 10.24874/ti.1674.05.24.07

Tribology in Industry

www.tribology.rs

RESEARCH

Optimization and Analysis of Dry Sliding Wear Behavior of AlCrTiSiN Coated SKD61 Steel Using Response Surface Methodology

Yupin Supachoke[a,*], Sutham Siwawut[b], Parinya Srisattayakul[b], Piyapong Kumkoon[b], Kessinee Ngaohiranpat[c]

[a]*Department of Engineering, Faculty of Engineering, Rajamangala University of Technology Krungthep, Bangkok, 10120, Thailand,*
[b]*Department of Industrial Engineering, Faculty of Engineering, Rajamangala University of Technology Krungthep, Bangkok, 10120, Thailand,*
[c]*NanoShield PVD Hard Coating Co., Ltd., Samutprakarn, 10560, Thailand.*

Keywords:

SKD61 steel
AlCrTiSiN
Filtered cathodic arc plasma
Response surface methodology
Sliding wear test
Wear rate

* Corresponding author:

Yupin Supachokea
E-mail:
649041610068@mail.rmutk.ac.th

Received: 1 May 2024
Revised: 1 June 2024
Accepted: 2 July 2024

A B S T R A C T

The aim of this research is to investigate the wear behavior of SKD61 steel coated with AlCrTiSiN using the Filtered cathodic arc plasma deposition coating method while adhering to VDI 3198 standards for coating adhesion assessment. Dry sliding wear tests, conducted according to ASTM G133-05. The experiment is designed using response surface methodology (RSM) to determine the response parameter as the wear rate, with independent parameters of interest including load, sliding velocity, and sliding distance ranging from 5 to 11N, 0.1 to 0.2 m/s, and 250 to 550 m, respectively. Additionally, wear characteristics are analyzed using SEM-EDS analysis. The wear test results demonstrate that load had the most significant impact on the wear rate, followed by distance and speed, respectively. The target of achieving minimal wear rate was attained with a load of 5 N, a sliding velocity of 0.11 m/s, and a sliding distance of 550 m. Model significance testing revealed that the determination coefficient (R^2) and adjusted determination coefficient values, indicating the accuracy of the model, were equal to 93.96% and 88.53%, respectively.

1. INTRODUCTION

The JIS SKD61 hot work tool steel is widely used in different industries, especially for stamping, extrusion, casting as well as other metal forming molds due to there is a chromium-bases content which enhanced high wear resistance, toughness level, mechanical properties, and good hardenability [1-3]. No matter how excellent the mechanical properties, there are several factors that limit the mold life whether the deterioration of the mold surface due to corrosion, abrasion, plastic deformation, and delamination etc [4-6].

Mold damage and defects disrupt production, especially considering the substantial expense of molds. As a result, soldering emerges as a prevalent method for repair, often involving the removal of protective layers such as coatings or lubricants, which is time-consuming for repairs [7]. To address these issues, numerous researchers are working to minimize die soldering. For instance, methods such as die treatment [8] and coating [9-10] have been explored. Han Qingyou and Viswanathan advocate that surface coating represents the most effective method for minimizing soldering [11].

Industries have developed various thin film coating techniques to enhance material lifespan and surface protection, such as Chemical Vapor Deposition (CVD) and Physical Vapor Deposition (PVD). PVD coating offers notable advantages, including low temperature deposition, zero generating pollution, and achieving high deposition rates [12]. The primary drawback of Arc-PVD coatings is the formation of micro droplets on the surface, a thermophysical process that takes place during the cathode spot of the vacuum arc. This phenomenon significantly impacts the properties and performance of the coating [13-14]. Filtered Cathodic Vacuum Arc Deposition (FCVAD) is a coating technique that has garnered significant attention in recent years. This is due to its capability to independently control the deposition rate and substrate temperature, without the need for gas arcing like other PVD processes [15-17]. The filter can be mitigating the occurrence of micro droplets during the coating process leads to an exceptionally smooth surface and finer grain structure, rendering it well-suited for applications demanding high surface quality [18]. Additionally, it has been reported that this technique can increase tool life [19-20].

The integration of nano materials, particularly Si and Cr, into coatings is highly intriguing because of their positive impact on mechanical properties and tribological enhancement [21]. Further studies on mechanical properties have revealed that TiAlCrSiN exhibits superior oxidation resistance and deformation resistance compared to TiAlCrN coating [21-22]. This is attributed to the crystallized Si atoms incorporated within the coating, which are embedded in an amorphous SiNx matrix. This configuration restrains the growth of columnar crystals and adjusts the grains, consequently increasing hardness [23-24]. Meanwhile, Siwawut et al. also found that the addition of Cr in coating, resulting in tools coated with CrTiAlSiN, exhibited better performance compared to those coated with TiAlSiN [25]. In the investigation of the tribological behavior during piston sliding tests of AlSiTiN, CrAlTiN, and CrAlSiTiN coatings, it was observed that the incorporation of Si was more effective in preventing wear compared to Cr. However, the combination of both Si and Cr demonstrated even better results, exhibiting the highest wear resistance [26].

The present study aims to analyze and optimize the impact of parameters related to dry sliding wear tests on the wear rate of AlCrTiSiN on JIS SKD61 steel using the response surface methodology (RSM). This approach is employed to develop a model that investigates the relationship between responses (wear behavior) and process parameters (load, sliding velocity, and sliding distance), aiming to enhance and optimize the response variable with least experimentation [27]. This study concentrates on examining the influential factors affecting groove wear, taking into account load, sliding distance, and sliding velocity through the utilization of the central composite design (CCD) experimental method.

2. MATERIAL AND METHOD

2.1 Materials

JIS SKD61 steel, measuring 25x40x10mm, possesses a composition in wt% of 0.365% C, 1.001% Si, 0.342% Mn, 0.02% P, 0.1% Cm, 5.028% Cr, 1.234% Mo, 0.84% V, and balance Fe.

The sample surfaces were sequentially polished with 600, 1000, and 1500 sandpaper, followed by polishing with a felt cloth at a speed of 600 rpm. Subsequently, these steels were hardened to a hardness of 52-55 HRC. The samples were positioned within a vacuum arc cathodic system housed within a furnace. Operating parameters were configured to set the apparatus at a temperature of 400°C and a based pressure maintained at 5×10^{-3} Pa. Initially, the Argon glow discharge cleaning was performed at 2.0 Pa. Following this, the metal plasma from Cr was

used for sputtering to cleanse the sample surface, effectively eliminating any impurities. A CrN interlayer was subsequently applied, followed by coating with AlCrTiSiN layer under a nitrogen atmosphere maintained at 1.5 Pa, with an applied bias of 100 V. Coating thickness was assessed using the Calotest machine, employing a spherical ball with a diameter of 30 mm. The ball was pressed and rotated onto the coating surface at a speed of 2,500 rpm for 60 s, followed by measurement using an optical microscope show in Fig. 1. The thickness of CrN interlayer and AlCrTiSiN coating layer was calculated to be 296 nm and 3.80 μm respectively.

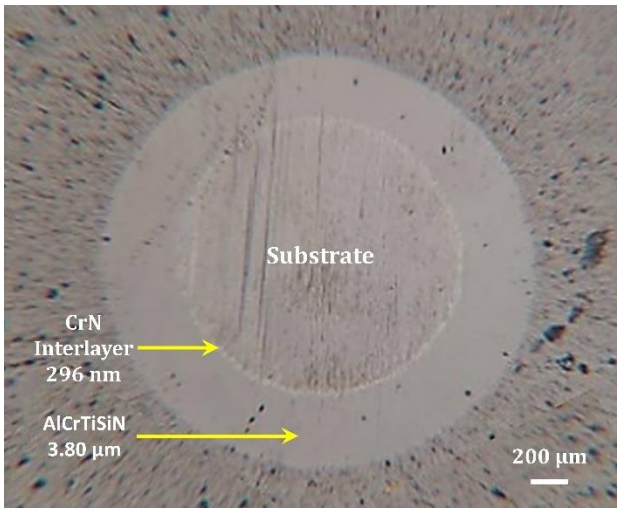

Fig. 1. AlCrTiSiN coating thickness.

The adhesion of the coating to the surface is evaluated according to VDI 3198 standard using a Rockwell-C indenter with a hardness tester applying load of 1471 N [28]. A sphere–conical diamond tip with 120 angular sides is used to assess radial cracks and deformation [29], and the results are compared with the VDI 3198 chart indentation test. This standard categorizes indentation adhesion into six categories HF1–HF6, with HF3 indicating acceptable adhesion [30]. Testing the adhesion of the AlCrTiSiN coating on SKD61 steel in Fig. 2 reveals slight circumferential cracks on the surface around the outer ring, however no signs of delamination are apparent. Based on this observation, the coating is estimated to possess high adhesion strength, corresponding to HF1.

2.2 Design of experiments

The dry sliding wear test was conducted following ASTM G133-05 standard [31], employing a tungsten carbide contact ball with a diameter of 6 mm and an amplitude of 10 mm. The experiment was designed using the Response Surface Methodology (RSM) technique to analyze the wear rate, employing a Central Composite Design (CCD) consisting of 20 experimental runs as shown in Table 1. Following each test, the samples were cleaned with acetone and dried. Subsequently, the weight loss was measured using a digital weighing scale with an accuracy of 0.0001 g. Data were collected three times, and the results were averaged to calculate the required wear rate of the composite material, as formular (1):

$$W = \frac{M}{\rho D} \quad (1)$$

Where 'W' represents the wear rate (mm^3/m), 'M' is weight loss (g), 'ρ' is density (g/mm^3), and 'D' is the sliding distance (m).

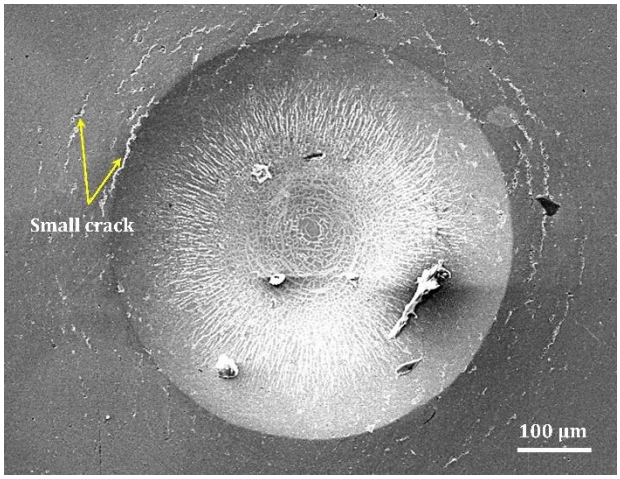

Fig. 2. The SEM image of the indentation trace in the sample.

3. RESULTS AND DISCUSSIONS

The effect of different parameters on the wear test of SKD61 steel surface coated with AlCrTiSiN, investigated using the RSM technique, are presented below.

3.1 Response surface model

The wear rate results for dry sliding tests, conducted according to the designed experiment, are presented. The response variable is expressed as the wear rate, while the independent factors are weight, scroll speed, and

scroll distance. The experimental results are displayed in Table 1. Normal probability assessment of the data for the wear rate depicted in Fig. 3 indicates that residuals exhibit linearity, suggesting normally distributed errors. Tests for independence were conducted by graphing residuals against run order, confirming the absence of discernible patterns attributable to residual distribution between levels.

Table 1. Experiments wear rates value of coated SKD61 steel.

S. No.	Load (N)	Sliding velocity (m/s)	Sliding distance (m)	Wear rate (mm^3/m) x 10^{-9}
1	11	0.15	400	1.699
2	6	0.12	300	0.406
3	6	0.18	300	0.471
4	6	0.12	500	0.052
5	6	0.18	500	0.770
6	10	0.12	300	1.667
7	10	0.18	300	1.069
8	10	0.12	500	2.194
9	10	0.18	500	1.488
10	5	0.15	400	0.257
11	8	0.1	400	1.507
12	8	0.2	400	1.379
13	8	0.15	250	0.693
14	8	0.15	550	1.283
15	8	0.15	400	0.810
16	8	0.15	400	0.706
17	8	0.15	400	0.770
18	8	0.15	400	0.768
19	8	0.15	400	0.805
20	8	0.15	400	0.802

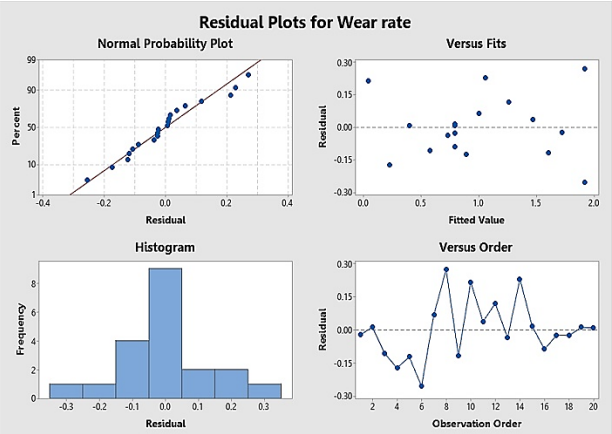

Fig. 3. Input data analysis of plot for wear rate.

Table 2 shows the estimated regression coefficients of the wear rate influenced by the parameters on the response variable, as indicated by the regression equation in Equation 2. From Table 2, it was evident that the most significant contributor to the wear rate is the load, compared to the sliding velocity and sliding distance. The significance test of the model revealed a determination coefficient (R^2) value of 93.96%, indicating the model's accuracy, and an adjusted determination coefficient value of 88.53%, signifying a strong relationship between the process parameters and the response variable.

$$\text{Wear rate} = 2.97 + 0.668\ \text{Load} - 50.1\ \text{Speed} - 0.01135\ \text{Distance} + 0.0098\ \text{Load*Load} + 228.5\ \text{Speed*Speed} + 0.000004\ \text{Distance*Distance} - 4.59\ \text{Load*Speed} + 0.000360\ \text{Load*Distance} + 0.0404\ \text{Speed*Distance} \quad (2)$$

Table 2. Significant test results for wear rate.

Term	Coef	SE Coef	T	P
Constant	0.7946	0.0743	10.70	0.000
Load	0.8399	0.0857	9.81	0.000
Speed	-0.1047	0.0908	-1.15	0.276
Distance	0.1621	0.0864	1.88	0.090
Load*Load	0.088	0.131	0.67	0.518
Speed*Speed	0.571	0.137	4.16	0.002
Distance*Distance	0.098	0.131	0.75	0.473
Load*Speed	-0.689	0.187	-3.69	0.004
Load*Distance	0.162	0.170	0.95	0.364
Speed*Distance	0.303	0.189	1.60	0.140

3.2 Analysis of variance

Analysis of variance for wear rates was conducted at a 95% confidence level and a 5% significance level, where significance was determined at a P-value less than 0.05. From Table 3, it can be concluded that the regression and linear model terms have the highest significance, followed by the interaction term, and square term, respectively. The calculated F-value remains greater than the P-value, confirming the adequacy of the model and its acceptance

Table 3. Analysis of variance for wear rate

Source	DF	F	P
Regression	9	17.30	0.000
Linear	3	32.22	0.000
Square	3	5.91	0.014
Interaction	3	7.84	0.006
Residual Error	10		
Lack-of-Fit	4	1.97	0.219
Pure Error	6		
Total	19		

3.3 Influence of process parameters on wear rate

Fig. 4 displays the contour diagram, illustrating the relationship between the wear rate, load, and sliding velocity. It reveals that as the applied load increases from 5 N to 11 N, the wear rate also increases. This occurs because greater loads lead to increased contact pressure and friction coefficient between the surfaces [32]. Consequently, elevated stress, leading to plastic deformation and eventual adhesion failure at the contact surface.

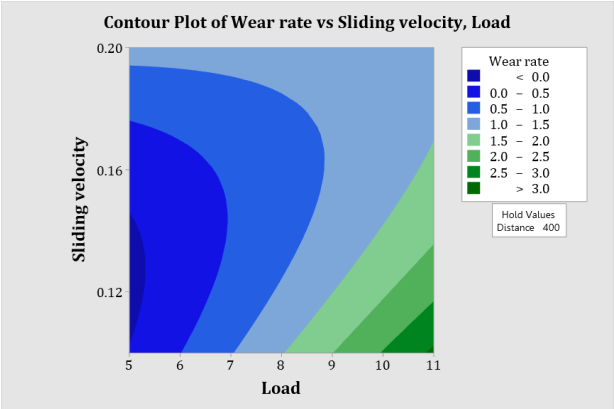

Fig. 4. Wear rate of contour plot in term of sliding velocity and load.

Scanning electron microscopy (SEM) analysis of Fig. 5a reveals that at a 6 N load, there is slight adhesive wear from previously loosened particles fragments. The adhesive coating begins to crack and detach, suggesting that the cracks in the adhesive wear area could lead to separation of the coating surface. In Fig. 5b, at a load of 10 N, it is evident that the surface of the specimen undergoes severe cracking, adhesion failure and micro-delamination. This occurs due to particles dislodged during sliding testing fused with the high-temperature surface, leading to adhesive wear and the roughening of the coating surface. After a certain duration of testing, particles adhered to the surface detach along with the coating layer, and the integrity of coating surface is compromised, thereby causing an accelerated rate of material removal, which is the primary cause of severe wear.

The EDS analysis of the abrasion area in Zone A and particle adhesion in Zone B (highlighted by the red frame in Fig. 5a) is depicted in Fig. 5c and Fig. 5d, respectively. In Zone A, the analysis reveals the following composition in wt% 5.3% Al, 53.5% Cr, 7.6% Ti, 0.6% Si and 15.4% N, while in Zone B, where particles adhere, the composition comprises in wt% 7.5% Al, 59% Cr, 12.8% Ti, 1.5% Si and 15.6% N. This confirms that the dislodged coating particles are fused to adhere to the coating.

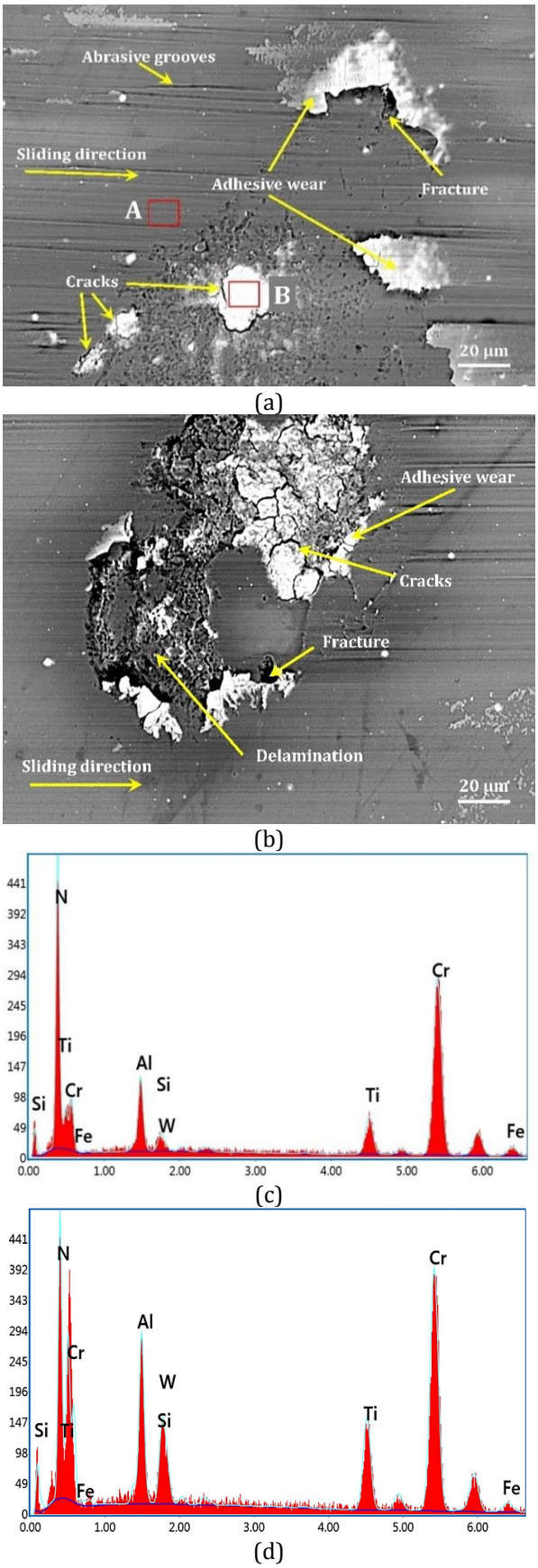

Fig. 5. Worn surface of specimen at different load (a) L=6 N, S=0.18 m/s, D=500 m, (b) L=10 N, S=0.18 m/s, D=500 m, (c) EDS spectrum of abrasive area (zone A), (d) EDS spectrum of adhering particle (zone B).

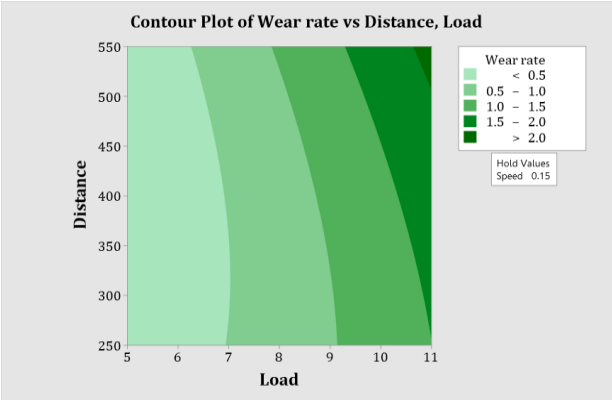

Fig. 6. Wear rate of contour plot in term of distance and load.

The impact of wear rate with varying sliding distances is illustrated in Fig. 6. At the initial load, it was observed that with increasing sliding distance, there was only a minor increase in the wear rate. This can be attributed to the effect of filtered cathodic arc plasma deposition coating, where filtration of micro droplets primarily prevents coating failure, resulting in improved surface quality [33]. It effectively reduced friction between the contact surfaces. However, as the load increases, the sliding distance starts to noticeably impact the wear rate. As observed in Fig. 7a and 7b, when the load and sliding velocity remain constant, an increase in sliding distance results in greater particle adhesion. Some areas start to display signs of cracking, particularly where the melted material adheres strongly. Eventually, the surface becomes unstable and experiences adhesive failure, causing the coating to separate from the substrate, forming micro holes.

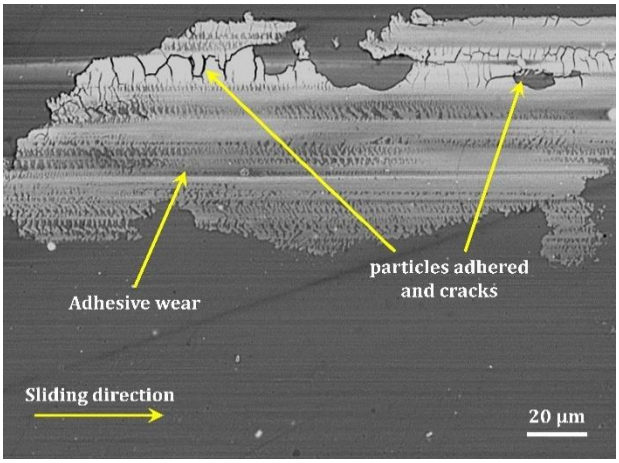

(a)

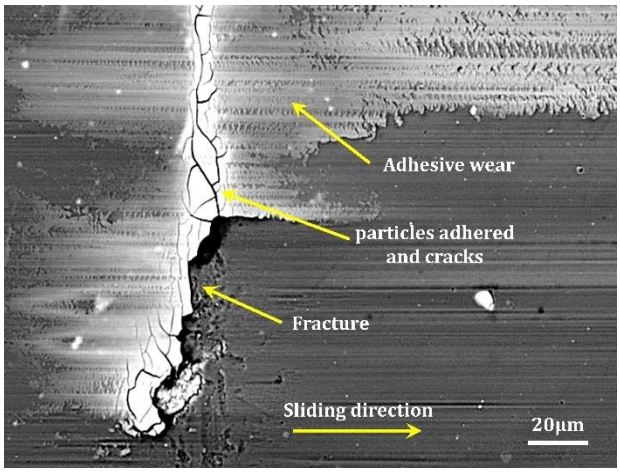

(b)

Fig. 7. Worn surface of specimen at different sliding distance (a) L=8 N, S=0.15 m/s, D=250 m, (b) L=8 N, S=0.15 m/s, D=550 m.

Figure 8 illustrates the impact of sliding speed and distance, revealing that at the lowest sliding velocity, a high wear rate occurs due to the elimination of sharp peaks, resulting in a smoother surface with subsequently lower contact stress. As the test distance increases, the wear rate gradually rises. Conversely, when the sliding speed is held constant, there is an observed increase in wear rate attributed to adhesive wear caused by particles dislodged during the test, which fuse onto the surface of the coating layer. Consequently, the coating layer thickens, as shown in Fig. 9b. It is evident that the particles adhering to the coating surface are distributed across a broader area compared to Fig. 9a, where the particles adhere and fracture along the sliding direction.

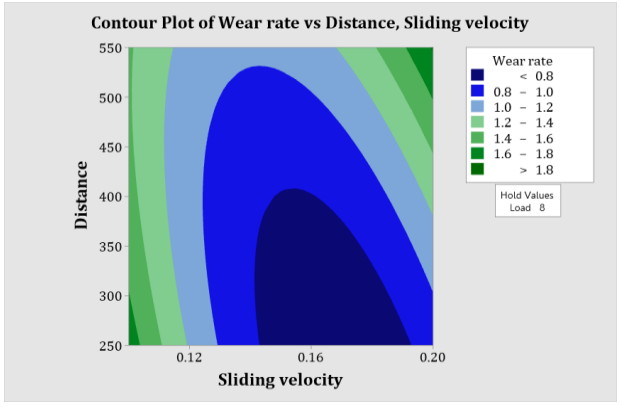

Fig. 8. Wear rate of contour plot in term of Distance and Sliding velocity.

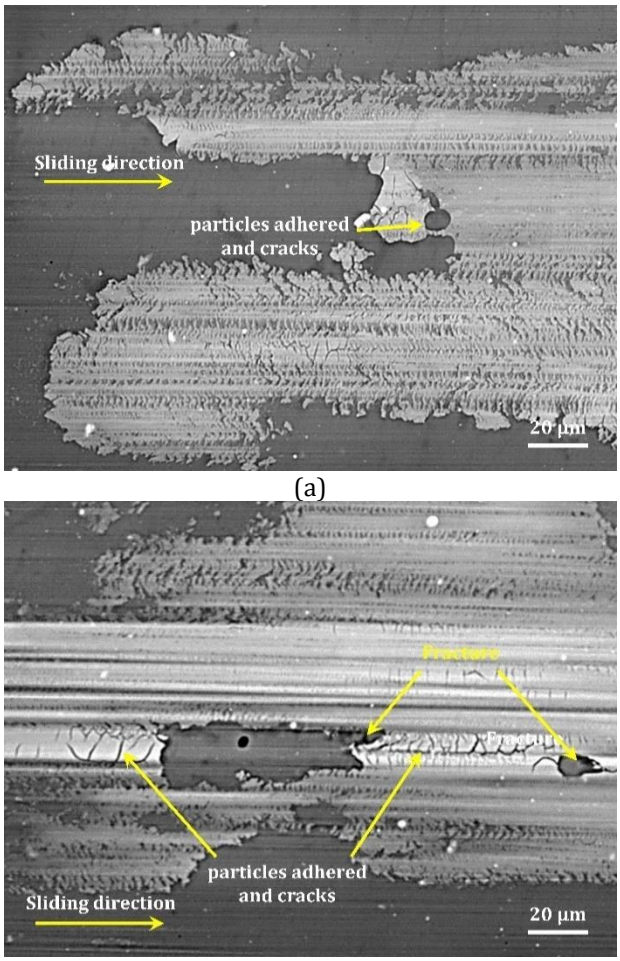

Fig. 9. Worn surface of specimen at different sliding velocity (a) L=8 N, S=0.10 m/s, D=400 m, (b) L=8 N, S=0.20 m/s, D=400 m.

3.4 Response optimization

Optimization utilizing the RSM technique aims to identify the optimal parameters which lead to lowest wear rate during the dry sliding wear test of AlCrTiSiN-coated SKD61 steel. The parameters of interest include load, sliding velocity, and sliding distance.

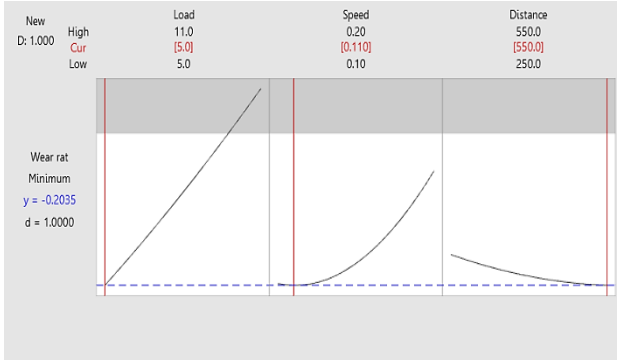

Fig. 10. Optimum values of process parameters achieved through RSM.

To achieve the target of an optimal load of 5 N, a sliding velocity of 0.11 m/s, and a sliding distance of 550 m, refer to Fig. 10

4. CONCLUSION

Investigation into the wear behavior of AlCrTiSiN coating deposited via Filtered cathodic arc plasma deposition process, with a coating thickness of 3.80 microns on SKD61 steel, utilizing response surface methodology to identify the optimal factors contributing to the lowest wear rate. The input parameters in the testing process include scanning electron microscopy analysis, as illustrated below.

- Dry sliding wear tests were conducted under various parameter conditions determined by mathematical equations and optimized values using RSM techniques. The target of achieving minimal wear rate was attained with a load of 5 N, a sliding speed of 0.11 m/s, and a sliding distance of 550 m.
- The study revealed that the parameter exerting the greatest effect on the wear rate in this process is load, attributed to the heavily loaded contact surfaces. As particles dislodge, they adhere densely, resulting in an uneven surface. Subsequently, when these particles detach, it leads to adhesion failure of the coating and substrate, causing the occurrence of micro holes.
- Regarding sliding distance, the wear rate tends to decrease gradually as adhesive wear occurs, leading to the thickening of the coating. However, with an increase in sliding distance, densely packed particles cause the surface to become rough and initiate cracking, resulting in adhesive wear micro holes.
- The comparison of sliding velocity with wear rate reveals that an increase in sliding velocity leads to lower material removal due to the adhesion of particles onto the coating layer.

ORCID iDs

Yupin Supachoke 0009-0003-2854-7542
Sutham Siwawut 0009-0003-0366-3387
Parinya Srisattayakul 0009-0005-1923-7221
Piyapong Kumkoon 0009-0005-2878-8308
Kessinee Ngaohiranpat 0009-0000-1842-8409

REFERENCES

[1] V. T. Le, "The influence of additive powder on machinability and surface integrity of SKD61 steel by EDM process," *Materials and Manufacturing Processes*, vol. 36, no. 9, pp. 1084–1098, Feb. 2021, doi: 10.1080/10426914.2021.1885710.

[2] B. Wang, X. Zhao, W. Li, M. Qin, and J. Gu, "Effect of nitrided-layer microstructure control on wear behavior of AISI H13 hot work die steel," *Applied Surface Science*, vol. 431, pp. 39–43, Feb. 2018, doi: 10.1016/j.apsusc.2017.03.185.

[3] S. Katoch, R. Sehgal, and V. Singh, "Wear behavior of differently cryogenically treated AISI H13 steel against cold work steel," *Proceedings of the Institution of Mechanical Engineers. Part E, Journal of Process Mechanical Engineering*, vol. 233, no. 2, pp. 292–305, Jun. 2018, doi: 10.1177/0954408918781621.

[4] Y. C. Chen and K. Nakata, "Evaluation of microstructure and mechanical properties in friction stir processed SKD61 tool steel," *Materials Characterization*, vol. 60, no. 12, pp. 1471–1475, Dec. 2009, doi: 10.1016/j.matchar.2009.07.004.

[5] M. V. Leite *et al.*, "Wear mechanisms and microstructure of pulsed plasma nitrided AISI H13 tool steel," *Wear*, vol. 269, no. 5–6, pp. 466–472, Jul. 2010, doi: 10.1016/j.wear.2010.04.037.

[6] J. Peng, Z. Zhu, and D. Su, "Sliding wear of nitrided and duplex coated H13 steel against aluminium alloy," *Tribology International*, vol. 129, pp. 232–238, Jan. 2019, doi: 10.1016/j.triboint.2018.08.017.

[7] Q.-Y. Han, "Mechanism of die soldering during aluminum die casting," *China Foundry/China Foundry*, vol. 12, no. 2, pp. 136–143, Mar. 2015.

[8] M. A. Mochtar and R. Aldila, "Die soldering behavior of H13 and CR-MO-V tool steel on die casting process on Nitriding-Shot pinning die surface treatment," *Materials Science Forum*, vol. 1000, pp. 381–390, Jul. 2020, doi: 10.4028/www.scientific.net/msf.1000.381.

[9] D. Kukuruzovic *et al.*, "Investigation of CrAlN coatings soldering resistance for high pressure Die casting tools," *SVC Annual Technical Conference Proceedings - Society of Vacuum Coaters.* Oct. 2018, doi: 10.14332/svc18.proc.0024.

[10] M. Serekpayeva, R. Niyazbekova, K. M. A. Azzam, E.-S. Negim, A. Yeleussizova, and A. Ibzhanova, "Investigation of the properties of metallurgical slags and dust of electro filters to obtain protective anticorrosive coatings," *International Journal of Technology*, vol. 13, no. 3, p. 544, Jul. 2022, doi: 10.14716/ijtech.v13i3.4214.

[11] Q. Han and S. Viswanathan, "Analysis of the mechanism of die soldering in aluminum die casting," *Metallurgical and Materials Transactions. A, Physical Metallurgy and Materials Science*, vol. 34, no. 1, pp. 139–146, Jan. 2003, doi: 10.1007/s11661-003-0215-9.

[12] Y. Li *et al.*, "Effect of buffer layer on oxidation and corrosion resistance of CrN coatings on Zr alloy prepared by FCVAD technology," *Surface & Coatings Technology/Surface and Coatings Technology*, vol. 448, p. 128942, Oct. 2022, doi: 10.1016/j.surfcoat.2022.128942.

[13] R. L. Boxman and S. Goldsmith, "Macroparticle contamination in cathodic arc coatings: generation, transport and control," *Surface & Coatings Technology/Surface and Coatings Technology*, vol. 52, no. 1, pp. 39–50, Mar. 1992, doi: 10.1016/0257-8972(92)90369-l.

[14] H. -D. Steffens, M. Mack, K. Moehwald, and K. Reichel, "Reduction of droplet emission in random arc technology," *Surface & Coatings Technology/Surface and Coatings Technology*, vol. 46, no. 1, pp. 65–74, May 1991, doi: 10.1016/0257-8972(91)90150-u.

[15] H. G. Benti, A. D. Woldeyohannes, and B. S. Yigezu, "Improving the Efficiency of Cutting Tools through Application of Filtered Cathodic Vacuum Arc Deposition Coating Techniques: A Review," *Advances in Materials Science and Engineering*, vol. 2022, pp. 1–17, May 2022, doi: 10.1155/2022/1450805.

[16] M. M. Viana, T. D. S. Mohallem, G. L. T. Nascimento, and N. D. S. Mohallem, "Nanocrystalline titanium oxide thin films prepared by sol-gel process," *Brazilian Journal of Physics*, vol. 36, no. 3b, pp. 1081–1083, Sep. 2006, doi: 10.1590/s0103-97332006000600075.

[17] R. Akhter, Z. Zhou, Z. Xie, and P. Munroe, "Enhancing the adhesion strength and wear resistance of nanostructured NiCrN coatings," *Applied Surface Science*, vol. 541, p. 148533, Mar. 2021, doi: 10.1016/j.apsusc.2020.148533.

[18] S. Ganeshkumar *et al.*, "Exploring the potential of nano technology: A assessment of nano-scale multi-layered-composite coatings for cutting tool performance," *Arabian Journal of Chemistry*, vol. 16, no. 10, p. 105173, Oct. 2023, doi: 10.1016/j.arabjc.2023.105173.

[19] A. A. Vereshchaka, A. S. Vereshchaka, O. Mgaloblishvili, M. N. Morgan, and A. D. Batako, "Nano-scale multilayered-composite coatings for the cutting tools,"*The International Journal of Advanced Manufacturing Technology/International Journal, Advanced Manufacturing Technology*, vol. 72, no. 1–4, pp. 303–317, Feb. 2014, doi: 10.1007/s00170-014-5673-2.

[20] J. Koskinen, "Cathodic-Arc and Thermal-Evaporation deposition," in *Elsevier eBooks*, 2014, pp. 3–55. doi: 10.1016/b978-0-08-096532-1.00409-x.

[21] S. K. Kim, P. Van Vinh, and J. W. Lee, "Deposition of superhard nanolayered TiCrAlSiN thin films by cathodic arc plasma deposition," *Surface & Coatings Technology/Surface and Coatings Technology*, vol. 202, no. 22–23, pp. 5395–5399, Aug. 2008, doi: 10.1016/j.surfcoat.2008.06.020.

[22] V. F. C. Sousa, F. J. G. Da Silva, G. F. Pinto, A. Baptista, and R. Alexandre, "Characteristics and wear Mechanisms of TIALN-Based Coatings for Machining Applications: A Comprehensive review," *Metals*, vol. 11, no. 2, p. 260, Feb. 2021, doi: 10.3390/met11020260.

[23] C.-C. Chang, H.-W. Chen, J.-W. Lee, and J.-G. Duh, "Influence of Si contents on tribological characteristics of CrAlSiN nanocomposite coatings," *Thin Solid Films*, vol. 584, pp. 46–51, Jun. 2015, doi: 10.1016/j.tsf.2015.02.022.

[24] Y.-C. Kuo, C.-J. Wang, and J.-W. Lee, "The microstructure and mechanical properties evaluation of CrTiAlSiN coatings: Effects of silicon content," *Thin Solid Films*, vol. 638, pp. 220–229, Sep. 2017, doi: 10.1016/j.tsf.2017.07.058.

[25] S. Siwawut, C. Saikaew, A. Wisitsoraat, and S. Surinphong, "Cutting performances and wear characteristics of WC inserts coated with TiAlSiN and CrTiAlSiN by filtered cathodic arc in dry face milling of cast iron," *˜the œInternational Journal of Advanced Manufacturing Technology/International Journal, Advanced Manufacturing Technology*, vol. 97, no. 9–12, pp. 3883–3892, Jun. 2018, doi: 10.1007/s00170-018-2200-x.

[26] H. P. Lim *et al.*, "A systematic investigation of the tribological behaviour of oxides formed on AlSiTiN, CrAlTiN, and CrAlSiTiN coatings," *Wear*, vol. 512–513, p. 204552, Jan. 2023, doi: 10.1016/j.wear.2022.204552.

[27] C. Aravind, S. Gopalakrishnan, and N. Radhika, "Investigating the adhesive wear properties of aluminum hybrid metal matrix composites at elevated temperatures using RSM technique," *Tribology in Industry*, vol. 41, no. 4, pp. 604–612, Dec. 2019, doi: 10.24874/ti.2019.41.04.12.

[28] Verein Deutscher Ingenieure Normen: VDI 3198. Dusseldorf, VDIVerlag, pp. 8, 1991.

[29] Y. Mahdavi, F. Qods, and B. Ghasemi, "Investigation of wear behavior of 34CRNIMO6 low alloy steel coated by PACVD method," *JOM*, vol. 76, no. 5, pp. 2189–2200, Mar. 2024, doi: 10.1007/s11837-024-06445-1.

[30] A. Gilewicz, R. Jedrzejewski, P. Myslinski, and B. Warcholinski, "Influence of substrate bias voltage on structure, morphology and mechanical properties of ALCRN coatings synthesized using Cathodic arc evaporation," *Tribology in Industry*, vol. 41, no. 4, pp. 484–497, Dec. 2019, doi: 10.24874/ti.2019.41.04.03.

[31] *Standard Test Method for Linearly Reciprocating Ball-on-Flat Sliding Wear*, ASTM G133-05, West Conshohocken, PA, USA, 2016, doi: 10.1520/G0133-05R16.

[32] A. Elhadi, A. Bouchoucha, W. Jomaa, Y. Zedan, T. Schmitt, and P. Bocher, "Study of surface wear and damage induced by dry sliding of tempered AISI 4140 steel against hardened AISI 1055 steel," *Tribology in Industry,* vol. 38, pp. 475-485, 2016.

[33] S. Rodríguez-Barrero, J. Fernández-Larrinoa, I. Azkona, L. N. L. De Lacalle, and R. Polvorosa, "Enhanced performance of nanostructured coatings for drilling by droplet elimination," *Materials and Manufacturing Processes*, vol. 31, no. 5, pp. 593–602, Oct. 2014, doi: 10.1080/10426914.2014.973582.